An Experimental Investigation of Robot Actuator Performance

Robert O. Ambrose, Delbert Tesar, Richard N. Hooper

University of Texas at Austin, Mechanical Engineering, Austin, Texas, USA 78712

Proceedings of the
Second International
Symposium on
Measurement and Control
in Robotics
ISMCR '92

November 15-19, 1992

AIST Tsukuba Research Center
Tsukuba Science City, Japan

IMEKO Technical Committee on Robotics (TC17)
Japan Industrial Robot Association (JIRA)
and
The Society of Instrument and Control Engineers of Japan (SICE)

Proceedings of the Second International Symposium on
Measurement and Control in Robotics (ISMCR '92)
Tsukuba Science City, Japan - November 15-19, 1992

An Experimental Investigation of Robot Actuator Performance

Robert O. Ambrose, Delbert Tesar, Richard N. Hooper

University of Texas at Austin, Mechanical Engineering, Austin, Texas, USA 78712

Abstract

Robot designers face the paradox of strength and response when selecting actuators for their systems. Within the actuators, motors, reducers, sensors and brakes all add inertia, compliance and friction to the drive trains. While some combinations of these components have been found to offer superior strength-to-weight ratios, they typically achieve this performance at the expense of dynamic response. The most demanding applications will be those that simultaneously require strength (high payloads), response (bandwidth) and a lightweight design. While over 40 criteria have been identified as significant in the selection of actuators [2], those that pertain specifically to the system's dynamic response are compliance, resistance, friction, inductance and inertia. These are recognized as the foundations of any electromechanical system, and are used as the basis for an experimental investigation of actuator performance for robotic applications.

Keywords: Design, Actuators, Dynamics

Introduction

The recent trend toward modular robot design is a response to manufacturing requirements for versatility on the factory floor. Non-manufacturing operations in space and other hazardous environments also require a broader spectrum of robot performance than possible with a single manipulator.

Actuators are a central technology that drives robot design, and thus offer a logical selection as the modular level of aggregation in robotic systems [2]. Defining the actuator as a prime building block in a robot architecture separates the power and performance issues of the servo systems from the kinematics and workspace issues associated with the robot's structural design [19].

Much work has been done at the kinematics level in modular robot design. The RMMS at CMU [19][20] and the CEBOT work by Fukuda of Japan [11] have forced their designers to formulate design methodologies for matching robot structures to specific tasks [16][12]. Beyond these kinematics methods, a robot's dynamic performance must also be matched to the mechanical requirements of a given task [2]. These requirements include an actuator's stiffness, friction, backlash, hysteresis, weight, torque, speed and bandwidth.

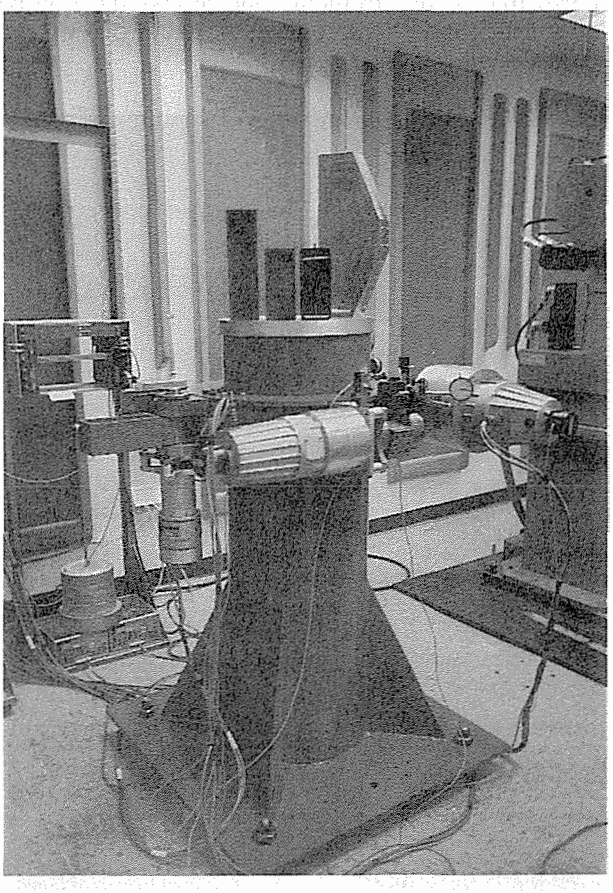

Figure 1 UT Modular Robotics Testbed

Experimental Approach

The goal here is to assess which combinations of servo components have the best dynamic response, and at what cost this performance

PR0003/92/0000-0623 © 1992 SICE

is achieved in terms of other criteria such as weight, volume, stiffness, friction, backlash, speed and payload. A mix of motor, reduction, sensor and controller technologies are contrasted, with recommendations for future robot actuator designs. Experiments augment this comparison using the actuator components available within the University of Texas Modular Robotics Testbed (UTMRT), shown in Figure 1, which is a research facility that is uniquely suited to this type of investigation. The performance of these existing components is investigated in a series of experiments, including:

- Joint Stiffness
- Link Stiffness
- Connection Stiffness
- Joint Backlash
- Joint Static Friction
- Joint Kinematic Friction
- Joint Bandwidth
- Joint Hysteresis

Manufacturers' data is used to add inertial properties, for assembling a lumped electromechanical model of a typical drive train [15][18]. The basic electromechanical properties of the servo system are then compared to the results from bandwidth experiments, where the system's open loop dynamic response is limited by some dominant pole [1]. An identification of which elements limit overall bandwidth will then be used to suggest new actuator designs for specific performance requirements and assess the relative strengths and weaknesses of each drive train component.

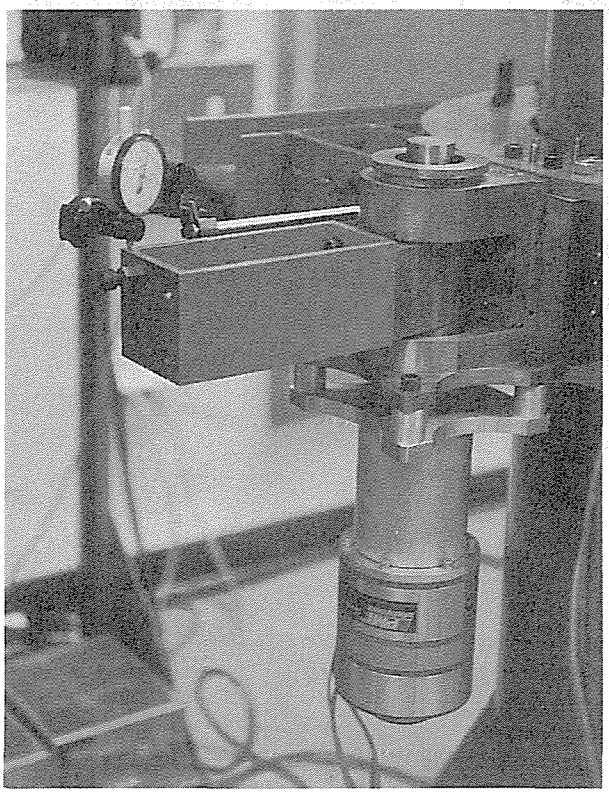

Figure 2 Isolated Joint Module

Five of the robotic joint modules available within the UTMRT were used for these experiments. Experiments were designed to focus on specific component attributes, such as the difference in stiction found in the drive types. The subsystems available within UTMRT for these experiments include:

- Digital Encoders
- 2 Pole Resolvers
- Tachometers
- Servo Disk Motors
- Servo Amplifiers
- Harmonic Drives
- Spur Gear Drives
- Electromechanical Brakes
- Brushless DC Motors
- Data Acquisition Systems

This investigation used the existing UTMRT digital controller, test stand, joint modules and link modules for the various experimental setups. In each case, combinations of actuator components were studied in isolation on one of the test stand's mounting sockets. Larger combinations of these modules assembled as robot manipulators have already been documented [2][13][19]. The next generation of robot modules, based on custom designed components rather than off-the-shelf technology, have recently been completed [8][14], and soon will be subjected to a similar set of tests for comparison.

Physical Setup

The robot joint and link modules built for UTMRT, one of which is shown in Figure 2, include structural yokes that allow for the connection of any of the available actuators for testing. As shown in Figure 2, these joints can be mounted on isolated test stand sockets for experimentation. Table 1 has a listing of performance criteria for each of these servo systems that were tested. Much of this data was acquired experimentally, as will be discussed in subsequent sections, and this table gives an overview of the scale of actuators considered in this study.

	PMI S6	PMI S9	PMI JR12	PMI JR16	Inland 6201
Continuous Torque (lb-ft)	26.6	42	93	262	25
Peak Torque (lb-ft)	290	410	925	2550	120
No Load Speed (rpm)	53	40	32	32	560
Mech. Time Constant (ms)	2.8	3.7	3.02	3.15	59
Elec. Time Constant (ms)	0.11	0.15	0.14	0.14	120
Actuator Inertia (oz-in-s-s)	0.0083	0.0206	0.0501	0.1811	1.46
Field Inductance (μH)	<100	<100	<100	<100	11,800
Field Resistance (Ω)	0.94	0.66	0.73	0.74	1.2
Length (in)	7.25	10	16	19	5.75
Maximum Diameter (in)	3.5	4.375	5.75	10	10
Weight (lb)	6.5	13.75	36	58	35

Table 1 Actuator Data

The two PMI JR series servo disk motors are equipped with REVEX spur gear drives with 100:1 speed ratios. Theses drives are typically 50% of the actuator system's weight. These two actuators are also equipped with fail-safe brakes, tachometers and relative digital encoders. The PMI S9 servo disk motor is equipped with an 80:1 harmonic reducer, a fail-safe brake, tachometer and relative digital

encoder. The PMI S6 servo disk motor is equipped with a 60:1 harmonic reducer, tachometer and relative digital encoder. The Inland RBE 6201 DC brushless motor is used as a direct drive. It is equipped with Hall Effect sensors and a 2 pole resolver.

Actuator Stiffness

In general, a six component load crosses any given robot joint, in the form of three forces and three moments. Depending on the joint's mobility (number of degrees of freedom, DOF), those loads will be transmitted as either reactions or actuations. For the case of an elbow joint, with one rotary DOF, the three forces and two of the moments are transmitted as reactions. The remaining moment is actuated through the joint's motor torque, or is left as zero in the case of a passive pin joint.

Since the reaction load paths cross fewer moving parts than the actuation load paths, it is not surprising that the stiffness associated with actuation is significantly lower than that of the reactions. Figure 3 shows experimental results that justify a more narrowed focus on the actuation stiffness. For Figure 3, the joint module shown in Figure 2 was mounted in isolation and loaded with weights that induced a moment about the actuated axis, with deformation readings made using a dial indicator positioned at the end of the link module. The deformation of the link module, which was measured separately [2], was subtracted as shown in the plot.

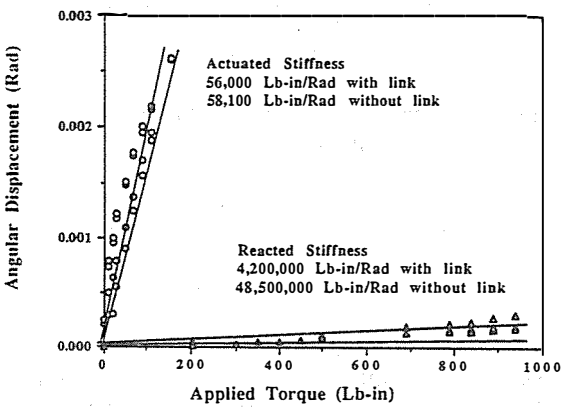

Figure 3 Actuated vs. Reacted Stiffness

The joint was then remounted with a twist so that its actuated axis was vertical. Subsequently applied loads induced a moment about the lateral reaction axis. Again the link deformation was subtracted, and the results show that the joint's reacted stiffness is approximately three orders of magnitude (10^3) greater than the actuated stiffness.

Figure 4 shows similar stiffness results for the PMI JR12 and JR16 actuators. The data is presented as a rotary stiffness that relates actuation torque levels to joint angle deflections. One interesting note is that while the JR16 has 2.75 times the torque rating of the JR12, it has only 50% greater stiffness. This suggests that actuator scaling is not a linear design operation. In fact, ratios for these two drives' torque, stiffness, friction, backlash, weight, diameter and length are all different.

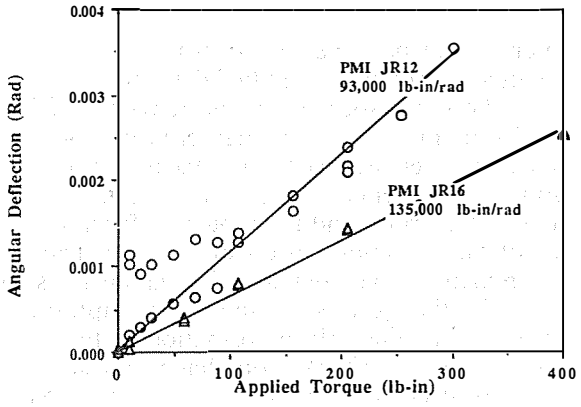

Figure 4 Stiffness Results for Spur Gears

Internal to the joint, two components were considered as the major contributors to the total compliance. The actuator shaft was found to have the most compliance. This analysis was based on the torsional analysis

$$K_{Shaft} = GJ/L \quad (1)$$

where

$$J = \pi d^4/32 = 0.031 \text{ in}^4 \quad (2)$$

$$G = 11.5 \times 10^6 \text{ psi} \quad (3)$$

so that

$$K_{Shaft} = 118{,}833 \text{ lb-in/rad} \quad (4)$$

which represents up to 55% of the compliance of the total joint's actuated deformation.

The second greatest source of compliance was identified as the shaft coupling, which was a square key. The 0.125" wide, 1.25" long square key was in shear with a predicted stiffness of

$$K_{Key} = T / \Phi \quad (5)$$

where T is the shaft torque and Φ is the angular displacement of the joint due to the key's compliance, which simplifies to

$$K_{Key} = Fd^2 / 4\delta \quad (6)$$

where F is the key force in the shear plane and δ is the linear deflection in that plane, with a diameter d. Using the stress strain relation for an elastic material

$$\sigma / \varepsilon = G = 8.0\, F / \delta \qquad (7)$$

for the given key dimensions. Solving for the linear deflection and substituting back into Eq. 6 results in

$$K_{Key} = Gd^2 / 32.0 = 202{,}000 \text{ lb-in/rad} \qquad (8)$$

which would be expected to produce 25% of the overall joint module's identified deflection.

Potential sources for the remaining 20% of the joint module's experimentally identified compliance were estimated to be the actual gearing or spline components in the reducers, the internal reduction bearings and the motor shaft on the input side of the reduction. A conclusive verification of this prediction would require subcomponent testing.

If the joint's actuation compliance is considered as the only deformation in the robotic structure, the end effector compliance of a six jointed robot constructed of joint and link modules will follow the form

$$\partial \underline{U} = [G^u_\phi]^T [C^u_\phi]\, [G^u_\phi]\, \underline{T}_u \qquad (9)$$

where

$$[C^u_\phi] = \begin{bmatrix} \frac{1}{K_1} & 0 & 0 & 0 & 0 & 0 \\ 0 & \frac{1}{K_2} & 0 & 0 & 0 & 0 \\ 0 & 0 & \frac{1}{K_3} & 0 & 0 & 0 \\ 0 & 0 & 0 & \frac{1}{K_4} & 0 & 0 \\ 0 & 0 & 0 & 0 & \frac{1}{K_5} & 0 \\ 0 & 0 & 0 & 0 & 0 & \frac{1}{K_6} \end{bmatrix} \qquad (10)$$

and each joint's experimentally measured actuation stiffness is known. A corollary expression for relating experimental stiffness of the joint to end effector stiffness is

$$\underline{T}_u = [G^u_\phi]^T [K^u_\phi]\, [G^u_\phi]\, \partial \underline{U} \qquad (11)$$

where the Jacobian has been taken in reverse order.

Actuator Friction

Robot actuators must operate in the low speed-high torque region of the power envelope. Consequently, drive specifications for efficiency are of little help in measuring friction effects on dynamic performance. Since efficiency is the power lost due to static friction (stiction) and kinematic friction (kiction) at some speed, manufacturers typically give efficiency ratings at high speed where the static friction is not significant. Some actuator applications, such as an automobile drive train, can tolerate high static frictions, if running friction is low enough to give good efficiency at some design speed. Robot's will typically have an average speed of zero, so efficiency is not a good metric for robot actuator performance.

A better approach is to measure stiction and kiction directly. Joint stiction will dominate a given arm's open loop force resolution, since low torque levels will dissipate into the drives and not pass through to the end effector. At some minimum torque rating, all drives will break free from stiction, and this level of torque, mapped through the arm, will limit the robot's force resolution. Stiction's electrical analogy would be a short circuit that occurs at some minimum threshold voltage. While feedback control strategies can be developed to help compensate for stiction, it still represents a fundamental actuator characteristic that is critical to robot performance.

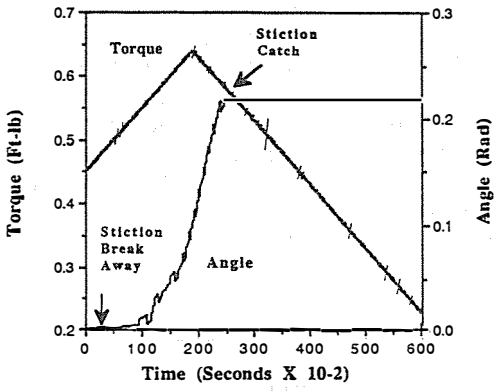

Figure 5 Friction for the PMI S9 Actuator with a Harmonic Drive

The UTMRT facility was used to test both stiction and kiction levels in three different drive types. The experimental protocol required a single joint mounted with a vertical actuated axis so that gravity did not induce a moment. The motor torque set point was gradually ramped up until the joint broke free from stiction, as identified by the encoder position feedback. Motor torque was then ramped down until the actuator was seized by kiction, which was found in all cases to occur at a lower torque level than stiction. Figure 5 shows the torque ramps and encoder positions for the PMI S9 harmonic drive. The torques at which the encoder registered the beginning and ending of angular movement are marked. These torques are defined as the actuators stiction and kiction.

An interesting effect with the harmonics was a relatively jagged break away, in contrast to the smooth, more viscous results found with the spur gear drives, as shown in Figures 6 and 7.

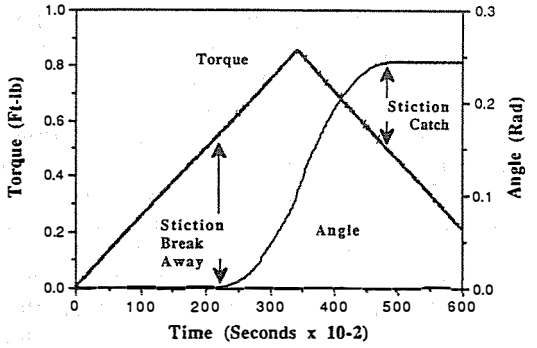

Figure 6 Friction for the PMI JR12 Actuator with a Spur Gear Drive

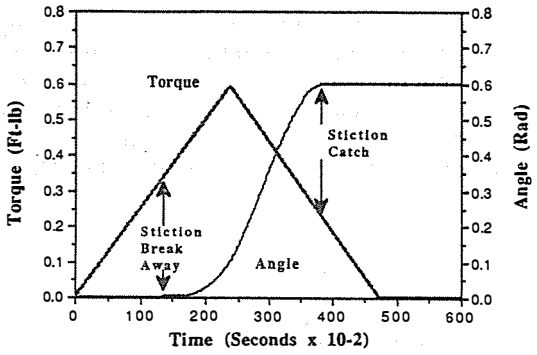

Figure 7 Friction for the PMI JR16 Actuator with a Spur Gear Drive

The torque required to break away from stiction was also more repeatable for the spur gear drives, as it was not position dependent. The harmonic was found to have angular positions where the stiction was significantly higher, possibly due to a damaged tooth on the drive's flexspline.

The harmonic drive's overall higher level of torque required to break the drive free from stiction is due to the preloaded nature of it's wave function generator, which was designed to minimize backlash, as shown in the next section. This is a clear example of the performance tradeoffs that robot designers must face. While the spur gear drive, with its precision bearings and case, is smoother, it achieves this performance at the expense of other characteristics such as weight and backlash.

An actuator's stiction manifests itself in the robot's performance by limiting the arm's open loop force resolution. The robot's open loop force resolution is a six component load that will be related to the joint's stiction torques by the relation

$$\underline{T}_u^F = -[G_\phi^u]^T \underline{T}_\phi^F \qquad (12)$$

where $\underline{T}_\phi^F$ is the vector of experimentally measured stiction torques for the robot's actuators. Due to the non linearity of the Jacobian, this friction limitation will vary across the arm's workspace, or as the arm is reconfigured with additional joint and link modules. The robotic system can be improved with a feedforward model, using the above relation, and a closed feedback loop using a six axis load cell mounted on the arm's end effector.

Actuator Backlash and Hysteresis

Within the drive elements of any mechanical reducer, the form of the contacts in the load path will impact the system's stiffness, backlash and friction. A preloaded contact will reduce backlash for a given frequency regime, but at the same time induce periodicity into the drive's friction and non linearity into the actuator's stiffness. The harmonic and spur gear drives studied here represent two alternatives in this design tradeoff.

The experimental protocol for the backlash experiments required each actuator to be mounted in a joint yoke with a vertical axis of mobility. A 7" link module was mounted to the joint's distal socket, producing a 9.25" lever arm. Loads were applied tangential to the link and linear deflections were measured with a dial indicator. The loading was then reduced and reversed, producing a hysteresis loop that also captured backlash at the zero load point. Data for the three PMI actuators is shown in Figure 8.

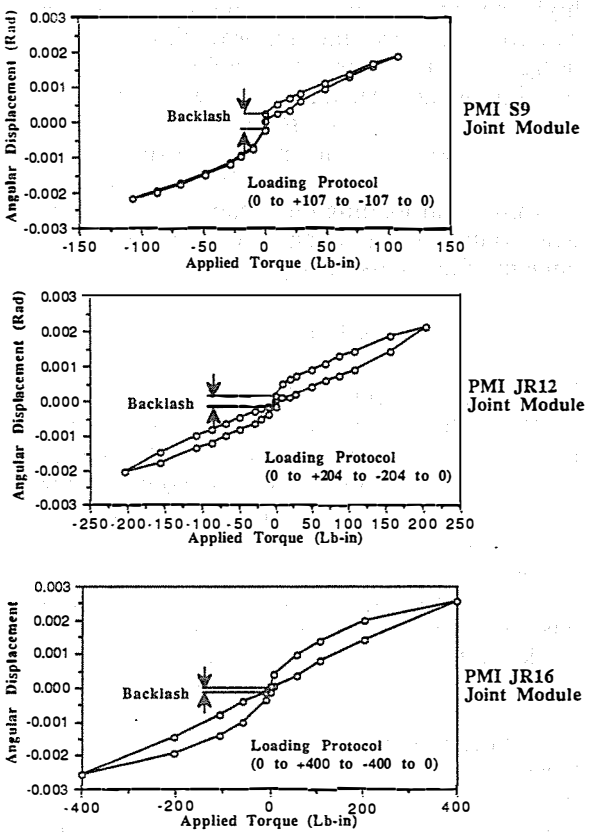

Figure 8 Hysteresis and Backlash Results

Backlash was also measured about the two reaction axis of the joint, and found to be below the instrumental resolution, which is at least two orders of magnitude (10^2) better than that of the actuated load path. If only the backlash of the actuators is considered, the error at the end effector of an arm assembled from these modular joints would be related to the joint backlash in the form

$$\partial \underline{U}_B = [G^u_\phi]\, \underline{\Phi}_B \qquad (13)$$

where $\underline{\Phi}_B$ is the vector of experimentally measured actuator backlashes. Even though control methods have been developed to reduce the problems associated with backlash, it remains a central design characteristic that must be faced when selecting robot drives, as these control methods are far from perfect.

Actuator Weight and Geometry

An actuator's weight and geometry will impact the entirety of a robot's design. The weight of distal joints and links will be a driving constraint for the payloads of proximal joints. Likewise, actuators with long aspect ratios will require design compromises in the links, yokes and connection sockets of a modular robot's design.

In terms of weight, the harmonic reducer is well designed. Its paradoxical kinematics deliver a high speed ratio with a minimum of drive elements. The loading is symmetric, providing balance in the design and minimizing structural material. The result is a light weight package that is well suited to higher speed DC brush and brushless motors.

In contrast, the spur gear drive has a heavy case design that is required to balance the asymmetrical loading characteristics of simple spur gear contact, where a radial force proportional to the tangent of the pressure angle and tangential force

$$F_r = F_t \tan \Phi_p \qquad (14)$$

that is felt at the center of each gear. Another reason for the higher relative weight of the spur gear design is that the higher precision, and consequently heavier, bearing mounts were intended to offer lower friction due to misalignment or deflection errors. The harmonic's light weight is clearly at the expense of friction.

In terms of geometry, the spur gear design has a shorter aspect ratio, since the gear surfaces are hardened to require a shorter gear face. Even though two 10:1 stages are required to achieve the 100:1 overall reduction, the spur gear drive's aspect ratio is still shorter than that of the harmonic. Since the harmonic's teeth are mounted on a flexible spline, they are less stiff, and thus require a longer tooth face to bear the load. This requires an overall longer aspect ratio for the drive's design.

It should be noted that these longer aspect ratios are a greater design constraint in the yoked, or elbow type joints, often dictating joint, link and thus arm diameter. An actuator's diameter will limit the yoked joint module's connection to connection distance, which should be minimized to allow the selected link modules to govern arm reach. Realistically, all yoked joints will have some proximal and distal link length, and in the joints designed for UTMRT, that total distance is 5". Joints with an in-line rotational kinematic structure will be limited more by actuator diameter, though length will still limit the minimum axial link length between such joints.

Actuator Bandwidth

An actuator's ability to track a velocity signal of a given frequency content is measured as the system's bandwidth. This is the quintessential measure of an actuator's dynamic performance, as it will be impacted by the actuator's friction, inertia and stiffness, electrical resistance and field inductance.

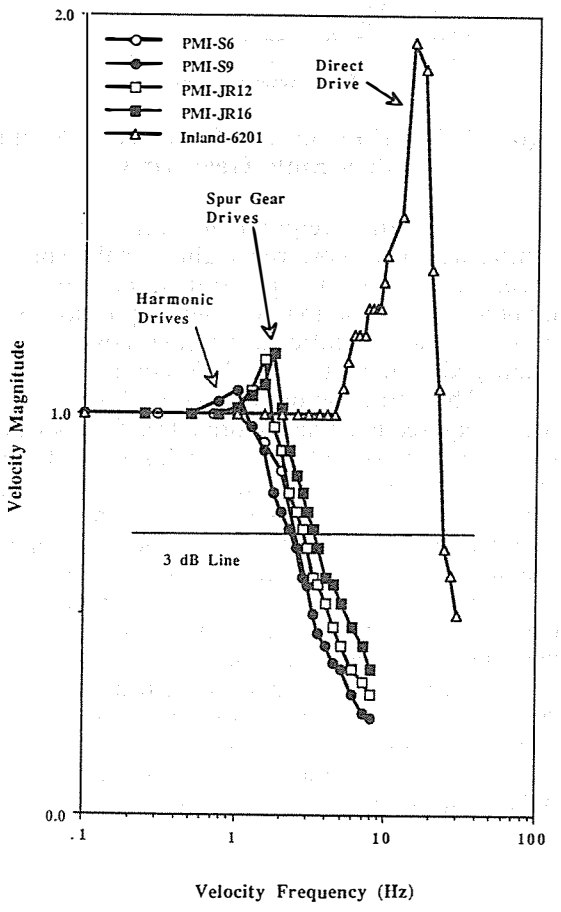

Figure 9 Experimental Bandwidth Results

The experimental protocol used for this test required that each actuator be mounted to the test stand in isolation and driven by a wave function generator. The actuator controllers were switched into a velocity control mode, where the motor speed is driven proportional to the ±10 volt set point delivered by the function generator.

A sinusoidal velocity set point was delivered with a 1 volt amplitude. The frequency of the command was increased, with velocity tracking data recorded on an oscilloscope connected to the tachometer or velocity probe. Bandwidth was defined as the frequency at which the velocity tracking amplitude rolled off by 3 dB. Figure 9 shows the Bode plot of the four PMI motors with reduction and the Inland motor used as a direct drive.

The most striking feature of the bandwidth plot is that actuators are grouped in frequency by drive type. This correlation holds true despite the broad class of powers considered. Even though the Inland 6201 is rated at over 3 Hp, its servo bandwidth is by far the best by a factor of 7. This result is due to its direct drive design [4], which has a better combination of inertia, friction, stiffness, inductance and resistance than the smaller, but reduced drives. Even though the two actuators with spur gear drives vary in power by a factor of three, their dynamic response is almost identical.

If considering motors alone, the PMI motors, especially the S series, have vastly better dynamic performance than the Inland design, with lower rotor inertia and inductance. The added inertia and compliance in the mechanical reducers moves the lower pole in the transfer function into a lower frequency range. The motor's transfer function will follow the form

$$G_M(s) = \frac{\frac{1}{K_E}}{[s\,t_m + 1]\,[s\,t_e + 1]} \qquad (15)$$

$$\left.\begin{aligned} t_m &= \frac{RJ}{K_E\,K_T} \\ t_e &= \frac{L}{R} \end{aligned}\right\} \; t_m >> t_e \qquad (16)$$

where these terms are defined as

K_E = Back EMF Constant
K_T = Torque Constant
J = Motor Rotor Inertia
t_m = Mechanical Time Constant
R = Field Resistance
t_e = Electrical Time Constant
L = Field Inductance

The addition of a drive to this model will impact only the motor rotor inertia, since motor features remain unchanged [1]. More likely, the drive will add both an inertia and compliance term, producing a third natural frequency that is the dominant pole. The drive behaves like a low pass filter, which does not transmit the high frequency motion of the motors.

A second feature of Figure 9 is the relative damping of the actuators, which also correlates with drive type, despite the scale of torque or power. As would be expected, the direct drive is most under damped, enabling it's controller to damp electronically when needed. The harmonic drives were most damped, which fits well with their experimentally measured higher friction levels. The spur gear drives had a lower damping than the harmonics, but much more than the direct drive.

Temperature will have an effect on both time constants in Eq. 15 by altering field resistance. As temperature increases, the field's electrical resistance will increase. This will increase the actuator's mechanical and electrical time constants.

Conclusions

Several types of robot drive trains were considered. Two sizes of harmonic reducers, two sizes of spur gear drives and a direct drive motor were investigated, all with a mixture of sensor and controller technologies. In each case, the reducer type was found to dominate the system's frequency response more than any other criteria, including the motor's electromechanical geometry and power. Experimentally identified values for stiffness, friction, bandwidth and backlash were considered relative to actuator power and stall torque ratings [2].

The observation that the reducer's design dominates the actuator's performance (stiffness, backlash, inertia, friction and bandwidth) is now being recognized in the design of new robot actuators [14], where the focus is on drive type. A modular approach is recommended to allow the designer to match the specific task requirements to the realistic limits of the existing component technologies [2][6][13].

Bibliography

[1] Ambrose, Catherine G., "Computer Aided Synthesis of Modular, Reconfigurable Robotic Controller Architectures", Ph.D. Dissertation, University of Texas at Austin, December 1992.

[2] Ambrose, Robert O.., "Design, Construction and Demonstration of Modular, Reconfigurable Robots", Ph.D. Dissertation, University of Texas at Austin, Aug, 1991.

[3] Ambrose, Robert O. and Tesar, D.,"Modular Robot Connection Design", *ASME Design 92, Fourth ASME Conference on Flexible Assembly Systems*, Scottsdale, Az, September 13-16, 1992.

[4] Asada, H., "Direct Drive Robots", MIT Press, 1987.

[5] Benhabib, B., Cohen, R., and Lipton, M.G., "Design of a Rotary-Joint-Based Modular Robot", *ASME Mechanisms Conference,* 1990.

[6] Butler, M. S., "An Applications-Based Assessment for Future Robot Development", Master's Thesis, University of Texas at Austin, 1991.

[7] Butler, P., Babcock, S., et. al., "The Laboratory Telerobotic Manipulator Program", OakRidge National Lab, 1989.

[8] Chu, Mars, "Design of a Structural Robotic One Degree of Freedom Elbow Module" , Master's Thesis, University of Texas at Austin, 1992

[9] Freeman, R.A. and Tesar, D., "The Generalized Coordinate Selection for the Dynamics of Complex Planar Mechanical Systems", *ASME Journal of Mechanical Design,* January 1982, 104:206-217.

[10] Fukuda, T., Toshio and Nakagawa, Seiya,"A Position Sensor Based Torque Control Method for a DC Motor with Reduction Gears", *IEEE Journal of Robotics and Automation,* 1987.

[11] Fukuda, T., Nakagawa and Kawauchi, "Self Organizing Robots Based on Cell Structures - CEBOT", *Proceedings of the IEEE International Workshop on Intelligent Robots and Systems, Tokyo, Japan,* 1988.

[12] Fukuda, T., Hosokai, H., Kawauchi, Y. and Buss, M., "Dynamically Reconfigurable Robotic System (DRRS) System Configuration and Implementation as CEBOT", *Proceedings of the IEEE Conferance on Robotics and Automation,* 1988.

[13] Hooper, R. N., "The Interactive Assembly and Computer Animation of Reconfigurable Robotic Systems", Master's Thesis, University of Texas at Austin, December, 1990.

[14] Iaconnis, J.,"Design and Prototype Development of Robot Actuator Modules", Master's Thesis, University of Texas at Austin, December, 1991.

[15] Inland Motors, Motor Catalog, 1991.

[16] Krishnan, A. and Khosla, P., "A Methodology to Determine the Dynamic Configuration of a Reconfigurable Manipulator", *The International First Symposium on Measurement and Control in Robotics,* 1990.

[17] Muller, H.W., "Epicyclic Drive Trains: Analysis, Synthesis and Application", Wayne State Press, Detroit, 1982.

[18] PMI Motion Technologies, Motor Catalog, 1990.

[19] Schmitz, D. and Kanade, T.," Design of a Reconfigurable Modular Manipulator System", Carnegie-Mellon University, 1988.

[20] Schmitz, D., Khosla, P. and Kanade, T., "The CMU Reconfigurable Modular Manipulator System", Technical Report, Carnegie Mellon University, CMU-RI-TR-88-7, 1988.

[21] Tesar, D. and Butler, M.S., "A Generalized Modular Architecture for Robotic Structure", *Manufacturing Reveiw,* Vol 2, June 1989, pp 91-117.